biomass_ipm Angle of internal friction and inter-particle friction coefficient

James C. Slosson, Yiming Li, Sena Atsyo, Heather Burkholder, and Hojae Yi

December 5, 2024

Abstract

Corn stover interactions involving cob fractions were found to contain the largest peaks and variance in friction coefficients (Table 3). Cob particles with woody-ring sub-fractions on the contacting surface were observed to be significantly harder and 'claw-like' in nature. Whereas the pith region of the cob was very similar to the exposed pith in stalk particles. Particles of stalk and husk both showed moderate friction coefficients.

From the observation that particles of corn cob show a larger standard deviation in the determined coefficient of friction, it can be hypothesized that particles of corn cob will have a high contribution to an erratic feedstock flow behavior. It can also be hypothesized that the cob will generate high frictional forces considering the high cohesive forces and moderate friction coefficients observed in a corn cob. The experimental data suggest that high-stress feedstock handling applications may be more stable with the removal of corn cob.

The anatomical fractions discussed in this paper were categorized using macro-observations for the purpose of potential mechanical separation. Under further review, it appears each corn stover fraction contained an associated set of sub-fractions that could be found in at least one other fraction. Sub-fractions could be generally characterized as woody, pithy, or leafy. Additional steps in comminuting particles to expose 'sub-fractions' may allow fluid separation techniques to create more uniform and, therefore, desirable products. It is recommended to repeat this experiment using two additional comminution methods (i.e., knife mill and hammer mill) practiced in the industry to study varying effects of size reduction equipment on friction coefficients.

1 Introduction

Department of Energy's Bioenergy Technology Office (BETO) considers corn stover a key candidate as a biomass source for its abundance and current use in integrated biorefineries (IBR) [1–4]. Corn stover refers to the remaining corn plant fractions (i.e., stalk, husk, and cob) after the lower stalk is cut away and the grain has been harvested. While many want to bring the advantages of new biofuel technologies to industrial production, there is a significant financial risk due to frequent misrepresentation of physical and chemical variabilities in effective lignocellulosic biomass handling and feeding [5–7]. In the most recent 2016 evaluation, total biofuel production only reached 7% of the expected 58 billion gallons per year design capacity [8]. The challenges in the handling of biomass are one of the crucial impediments to adopting biomass as feedstocks for biofuel production.

BETO [9] reports that flowability challenges are mainly associated with biomass density, particle size distribution, moisture content, angle of repose, shear stress, bridging tendency, cohesive strength, and friction of equipment surfaces [8]. The variations in biomass factors such as shape, size, moisture content, and low bulk density are considered to make it challenging to handle and transport in its original form [10].

The root cause of such variations in bulk behavior of milled biomass originates from the multiscale-nature as depicted in the Figure 1. This means in order to develop a first-principle based understanding of bulk biomass behavior, quantitative knowledge of interactions between particles is necessary. With such knowledge, one can investigate and develop a predictive model of the mechanical behavior of bulk biomass.

However, the majority of the metrics used for the mentioned flow challenges are focused on bulk behavior and do not address the inter-particle mechanics leading to bulk observation.

- Janssen's equation Janssen [11] and stresses on silo wallSchulze and Schwedes [12]
- Still not quantified Reynolds' question on the relationship between the angle of repose and friction between particles Reynolds [13]
- Recent studies with DEM still relying on fitted parameters that are not

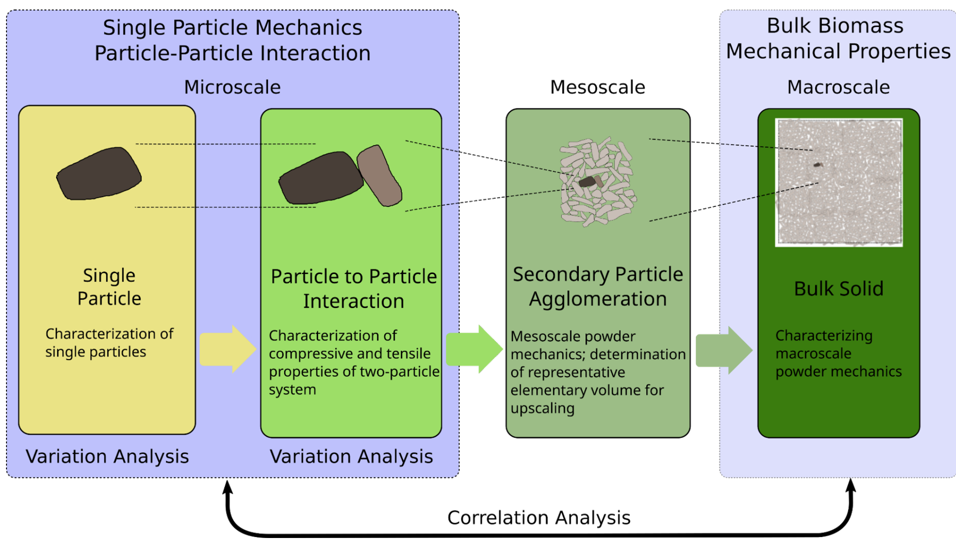

Figure 1: Schematic of the emerging bulk mechanical properties from the mechanical interactions between biomass particles to the bulk mechanical behavior of milled biomass

determined with particles Xia et al. [14] and F. Chen et al. [15, 16]

Understanding interparticle mechanics associated with each corn stover fraction will provide valuable information for understanding the overall poor flow behavior of milled corn stover. More specifically, such quantitative information will help identify certain fractions that may be significantly responsible for the poor flowability behavior of comingled corn stover fractions.

There exists a ASTM standards concerning the measuring friction coefficient including ASTM G115-10 [17]. However, listed methods in ASTM G115-10 [17] assumes a specific geometry, e.g., flat surface or sphere, and not feasible to implement for testing milled biomass particles, which are much smaller in size and irregular in shape. Also test protocols reflects repeated sliding in cyclic motion or rotation, which is implemented in a typical tribometer. This also reflects specific industrial applications such as ball bearing or sliding frames, which are not applicable to the interactions of biomass particles relevant to the bulk biomass flow.

- In other words, the current friction measurements focus on interactions between sliding surfaces, e.g., bearing. This focus is also reflected in the DEM framework, requiring sliding and rolling friction coefficient. From the perspective of the handling bulk biomass, or any other cohesive particulate materials, the friction coefficient of incipient relative motion between particle is of interest.

Therefore, we developed an in-house instrument and protocol that can determine mechanical interaction between biomass particles following the Derjaguin's adhesive friction model [18–20].

This study aims to gain quantitative knowledge of the interparticle mechanics of fractionated corn stover through the development of an interparticle mechanics tester capable of accommodating biomass particles and a test protocol to determine friction and adhesion properties. With the novel data on interparticle mechanical properties of corn stover particles from different anatomical origins, this study aims to examine the significance of the difference in friction coefficients between corn stover particles from different anatomical fractions. The knowledge gained by this study will contribute to reducing operational challenges by removing fractions with high friction and traction adhesion contributions.

1.1 Other notable quotes

K. L. Kenney et al., "Understanding biomass feedstock variability", Biofuels **4**, 111–127 (2013) page 121: Variability of biomass exceeds handling machinery design specification: This paper also mentions about the start-up or continuous running efficiency

2 Materials and Methods

This section details the method used to determine friction coefficients between anatomical fractions of corn stover.

Figure 2: Sample images of individual corn stover fractions used in the present study. 4mm cob Crumbles® (top left), 4mm husk Crumbles® (top right), 4mm stalk Crumbles® (bottom left), and 4mm leaf Crumbles® (bottom right)

2.1 Material Preprocessing History

A square bale of field-dried corn stover from Antares Corn Stover (Hardin, IO) was processed by Forest Concepts, LLC (Auburn, WA). The bale was hand separated and placed into labeled bins designated for each anatomical fraction. Individual fractions were then comminuted to Crumbles® using Forest Concepts' Crumbler® Rotary Shear technology and conveyed into a final screening process. The screening was performed using a 3-deck orbital screen to filter out fractions with geometric mean diameter outside the 4mm target.

Physical properties of particles of different tissue types of corn stover indicate that the crumbled particles are in consistent size (Table 1). However, the bulk density values are significantly different from each other (Wilcox test p = n.nn < 0.05).

Table 1: Physical properties of corn stover particles of different tissue type (Forest Concepts, LLC analytics laboratory in Auburn, WA).

Anatomical Fraction	**Moisture Content**	**Geometric Mean Diameter (mm)**		**Bulk Density (odkg/m^3)**	
	%MC wb	***Xgm***	***Sgm***	***Loose***	***Tapped***
Cob	9.7	6.6	1.6	179	217
Husk	9.7	4.6	1.6	48	66
Stalk	9.7	4.5	1.8	76	98

2.2 Particle size distribution

Corn Stover Fractions Cob shows distinctly different behavior with more material retained at larger sizes (4.75-5 mm) compared to other fractions1 Husk, leaf, stalk, and comingled fractions show similar PSD patterns with steep curves between 2-4 mm1 Most material across all fractions is retained between 2-5 mm opening sizes1 Southern Pine Residue Fractions Needle fraction shows significantly different behavior with most material passing through larger openings until 2.5 mm1 Bark, chip, and twig fractions exhibit similar PSD patterns1 More uniform distribution across different size ranges compared to corn stover1 Implications Processing Efficiency The different PSD patterns between fractions suggest that separate processing conditions might be optimal for different plant parts Cob (corn stover) and needle (pine) fractions may require different handling strategies due to their distinct size distributions Material Properties The differences in PSD reflect the inherent structural differences between: Woody biomass (pine residue) with more rigid fiber structure Herbaceous biomass (corn stover) with more flexible fiber arrangement Downstream Applications The varying particle size distributions could affect: Bulk density and flowability in storage and handling Surface area available for biological or chemical conversion Heat and mass transfer in thermochemical conversion processes This understanding can help optimize processing parameters and downstream conversion processes for different biomass fractions.

Corn Stover Fractions Cob shows distinctly different behavior with more material retained at larger sizes (4.75-5 mm) compared to other fractions1 Husk, leaf, stalk, and comingled fractions show similar PSD patterns with steep curves between 2-4 mm1 Most material across all fractions is retained between 2-5 mm opening sizes1 Southern Pine Residue Fractions Needle fraction shows significantly different behavior with most material passing through larger openings until 2.5 mm1 Bark, chip, and twig fractions exhibit similar PSD patterns1 More uniform distribution across different size ranges compared to corn stover1 Implications Processing Efficiency The different PSD patterns between fractions suggest that separate processing conditions might be optimal for different plant parts Cob (corn stover) and needle (pine) fractions may require different handling strategies due to their distinct size distributions Material Properties The differences in PSD reflect the inherent structural differences between: Woody biomass (pine residue) with more rigid fiber structure Herbaceous biomass (corn stover) with more flexible fiber arrangement Downstream Applications The varying particle size distributions could affect: Bulk density and flowability in storage and handling Surface area available for biological or chemical conversion Heat and mass transfer in thermochemical conversion processes This understanding can help optimize processing parameters and downstream conversion processes for different biomass fractions.

2.3 Inter-particle Mechanics (IPM) Tester

Existing tribometer, similar to the instrument used in Z. Chen et al. [22], can be used in determining friction coefficient. However, because of the dimension of typical milled biomass particles, an additional attachment is needed.

In addition, the cyclic reciprocating movement is not simulating the frictional interaction between biomass particles during handling. Furthermore, this arrangement is not adequate to determine adhesive friction following Derjaguin's law [19, 23].

The development of a new Inter-particle Mechanics (IPM) was needed (Figure 2) to measure the traction force between a stationary and moving particle under a varying magnitude of normal load. This arrangement allows for one test run to produce multiple normal force and lateral force measurements and alleviates the requirement to conduct separate tests with different normal forces in a conventional friction tester [17, 24]. The development of the new design was essential for simulating any possible orientation of two interacting particles. This design allows collecting friction coefficients over multiple untested regions without resampling surfaces or replacing test particles between each repetition. With this design, it is also possible to prepare and condition multiple test samples, e.g., conduct friction experiments in an environment-controlled chamber at a different environmental relative humidity.

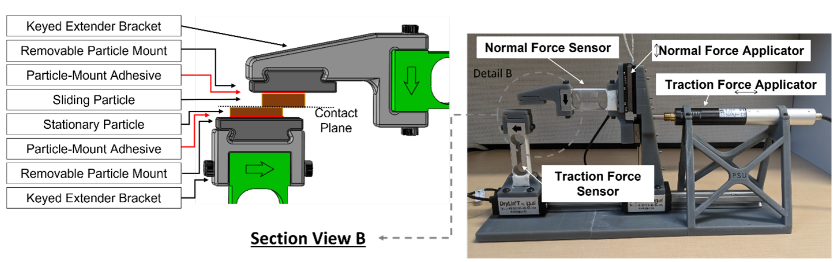

Figure 3: Inter-particle mechanics tester (right) with a detailed view of sample mounting (left).

2.4 Specifications and Operational Parameters of IPMT

An IPMT was developed to perform friction tests on fully supported particles, unsupported (over-hanging), or combinations of both. Sample holders and component position/capacity are easily adjustable to handle any particles of any size and shape. The specifications for the IPMT are limited to the following conditions.

- Minimum incremental push/pull motion is 0.05 µm.
- Maximum push/pull travel ranges up to 25 mm to accommodate a typical biomass particle size.
- Push/pull velocity is set to 1.2 mm/s.
- Maximum displacement of the normal force actuator is 14mm to accommodate a typical biomass particle size.
- Minimum normal displacement of the particle is as small as 6 nm.
- Three-dimensional control of the initial particle contact location is possible.
- Maximum allowed normal force is approximately 3 N.
- The accuracy of loadcell is ±0.02% of FS.
- Maximum sample rate is 1 kHz.

2.5 Experimental Design and Setup

An experimental procedure was developed to perform friction tests with minimal experimental error, as detailed below.

- Experimental Design A sample size of 12 was selected for each possible combination of anatomical fractions to obtain a minimum of three data points and to ensure the experiment could be completed as planned. Once all the data had been collected and analyzed, an analysis of variance ~~(ANOVA)~~ ($\alpha = 0.05$) was used to determine the source of variance. The Wilcoxon signed-rank (signed-rank) test was selected to test the null hypothesis (i.e., friction coefficients between corn stover particles from different anatomical fractions are not statistically different) for a population of unknown statistical distribution. The signed-rank test is a useful alternative to a paired student t-test when the normality of the observed data set is not ensured.

why?

- Sample Preparation Approximately 50 g samples were collected from each anatomical fraction of corn stover. Each sample was held in a controlled environment for 72 hours to allow for particles to reach equilibrium moisture content (~10% MCwb). Once particle moisture was equalized, particles were randomly selected and adhered to removable particle mounts (Figure 3) using Permatex *Ultra Bond™ Super Glue*. Mounting methods (fully vs. singly supported) and grain orientations were performed randomly with every particle. Conservative volumes of adhesives were applied to reduce absorption into particles as well as to ensure proper curing. A curing period of 24 hours (±2 h) (±2 hours) was established for experimental consistency.

Figure 4: Image of corn stover particles adhered to plastic particle mount for conditioning and testing. The upper and lower half of the image contains 4mm husk and cob fractions, respectively.

Once the adhesive had cured for 24 hours, particle pairs were randomly selected for testing. Table 2 contains the experimental plan for each possible particle pair and the required number of repetitions to be completed to test the null hypothesis.

- Inter-particle Mechanics test settings and operating Procedures Each experiment was performed at a sliding speed of 0.5 mm/min with a randomized initial normal loading force between 0.3 N and 2 N. Prior to each test, test operators must determine the required positioning of the normal

Table 2: Experimental plan for the required number of corn fraction test pairs and associated repetitions.

Base Particle	**Interacting Particle**	**Repetitions**
Cob	Cob	12
Cob	Husk	12
Cob	Leaf	12
Cob	Stalk	12
Husk	Husk	12
Husk	Leaf	12
Husk	Stalk	12
Leaf	Leaf	12
Leaf	Stalk	12
Stalk	Stalk	12

force applicator (Figure 3) to produce the target initial normal loading. This procedure was performed in less than 0.1mm increments to prevent overloading of the normal force sensor past the selected design capacity. Once the target initial normal force was applied, the traction force applicator and data collection were initiated. Data collection is terminated once particles are no longer in contact or upon sensor capacity concerns.

- Data collection and analysis methods Normal and traction force data were collected at 80Hz, using National Instruments™ LabVIEW and two 24-bit Di-1000U signal digitizers (Loadstar Sensors - Freemont, CA). The middle two quartiles were selected and extracted as steady-state data for further analysis for each data collection experiment performed.

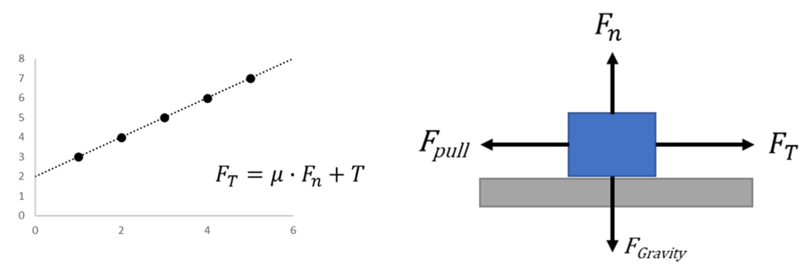

Figure 5: Theoretical plot of traction force versus normal force (Left). Force diagram of two particles (grey and blue) under applied normal and pulling force (Right).

Similar to as shown in Figure 5, the coefficient of friction (µ) will be determined using the average ratio of traction force to the applied normal force during steady-state conditions.

Variable	n	Min	q_1	$\widetilde{x}$	$\bar{x}$	q_3	Max	s	IQR	#NA
mu	20	0.194	0.221	0.250	0.258	0.288	0.394	0.051	0.067	0
c	20	-8.472	2.048	3.790	3.309	5.488	8.931	3.657	3.441	0

Table 4: Validation test results of polypropylene

3 Results and Discussion

3.1 Validation of the IPM

- reference material test: paper
- reference material test: polypropylene

Table 4 lists the results of the validation experiment.

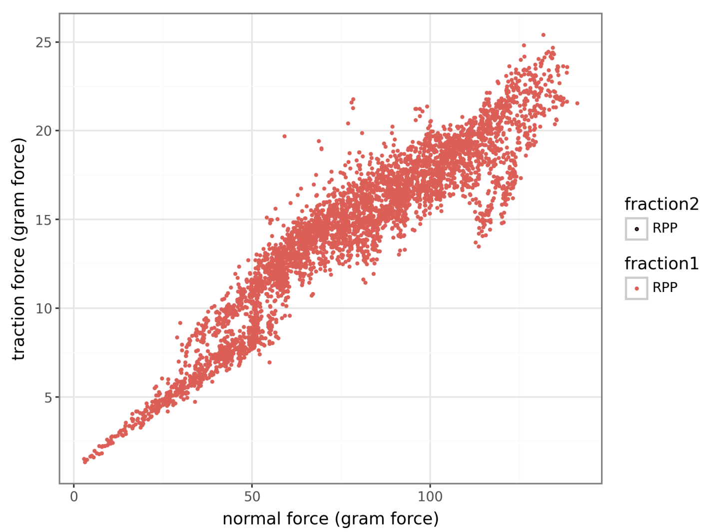

Figure 6: Validation test results of polyprophylene

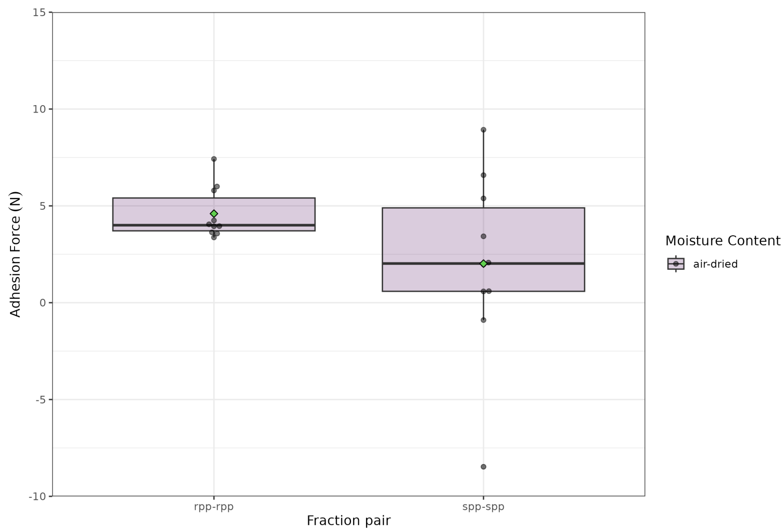

Figure 7: Validation test results of polyprophylene; adhesion force

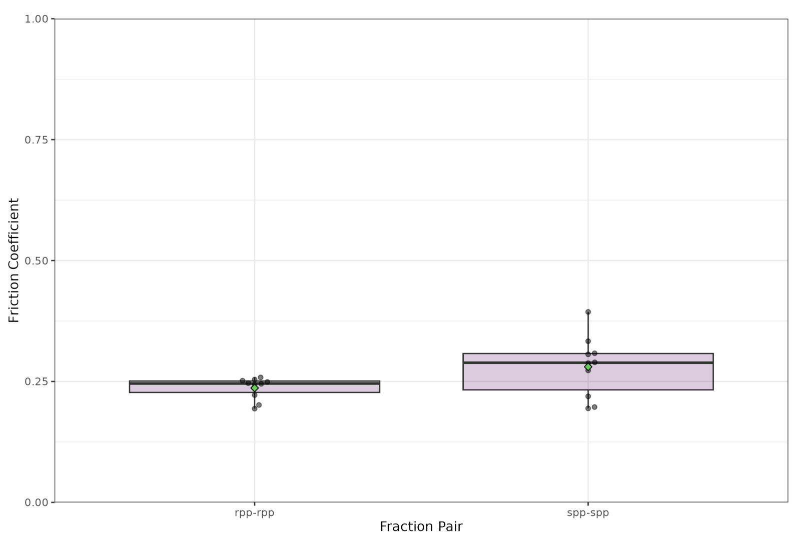

Figure 8: Validation test results of polyprophylene; friction coefficient

3.2 Corn stover particles from different tissue types

Corn stover interactions involving cob fractions were found to contain the largest peaks and variance in friction coefficients (Table 5). Cob particles with woody-ring sub-fractions on the contacting surface were observed to be significantly harder and 'claw-like' in nature. Whereas the pith region of the cob was very similar to the exposed pith in stalk particles. Particles of stalk and husk both showed moderate friction coefficients.

Table 5: Wilcox Signed Rank Test Critical Values Table

Paired Fractions	**Average Friction Coefficient**	**Standard Deviation**
stalk-stalk	0.28	0.09
cob-cob	0.86	0.26
husk-husk	0.23	0.06
stalk-cob	0.53	0.25
cob-husk	0.32	0.16
stalk-husk	0.21	0.07

An ANOVA test ($\alpha = 0.05$) showed the key source of variance in friction coefficients was found to be between different combinations of fractions. Leading to further investigation of key sources of variances. Without an understanding of the population distribution, a Wilcoxon signed-rank test was conducted to determine the significance across the variance with each corn stover fraction

Table 6: Anova test result

Particle Pair	**Comparison Pair**	**Sum<Cr?**	**Result**
stalk-stalk	cob-cob	TRUE	reject null
	husk-husk	FALSE	fail to reject
	stalk-cob	TRUE	reject null
	cob-husk	FALSE	fail to reject
	stalk-husk	FALSE	fail to reject
cob-cob	husk-husk	TRUE	reject null
	stalk-cob	TRUE	reject null
	cob-husk	TRUE	reject null
	stalk-husk	TRUE	reject null
husk-husk	stalk-cob	TRUE	reject null
	cob-husk	FALSE	fail to reject
	stalk-husk	FALSE	fail to reject
stalk-cob	cob-husk	FALSE	fail to reject
	stalk-husk	TRUE	reject null
cob-husk	stalk-husk	TRUE	reject null

combination. As shown in Table 6, the results suggest that cob fractions had a significantly different friction coefficient.

3.3 Friction coefficients and cohesion coefficient

- Mohr-Coulomb model

$$\tau = c + \sigma \tan \phi \tag{1}$$

  where τ is the shear stress, c is cohesion coefficient, σ is normal stress, and ϕ is the angle of internal friction

- Derjaguin's model

$$N_t = N_f + \mu N_n \tag{2}$$

  where N_f is the adhesion force, μ is the friction coefficient, and N_n is the normal force

These equations include definitions of adhesion/cohesion and friction coeffient at different scale, yet they convey similar connotation without a physical connection [13].

OR DO They?

Similar discussions can be made on Rankine/Janssen equation.

- Rankin's Rankine's lateral earth pressure theory, developed in 1857, is a fundamental model in geotechnical engineering used to analyze the pressure relationship between retaining walls and soil masses. This theory provides a stress field solution that predicts active and passive earth pressures under specific conditions.

$P_a \leftarrow K_a \gamma z - 2c\sqrt{K_a}$ $\quad$ $P_p = K_p \gamma z + 2c\sqrt{K_p}$

active lateral pressure $\quad$ passive lateral pressure

σ_3 σ_x σ_1 σ_z

real-world wall friction makes Rankine model overestimate active pressure, underestimate passive pressure

$K = \frac{\sigma_h}{\sigma_v} = \frac{\sigma_x}{\sigma_z} = \frac{\sigma_3}{\sigma_1}$

The theory is based on several key assumptions. It considers the soil to be isotropic and homogeneous, assumes an infinitely long wall (plane strain condition), and requires a planar ground surface (not necessarily level). Importantly, Rankine's model assumes no wall friction ($\delta = 0$) and sufficient wall movement to develop active or passive conditions.

Rankine's theory considers three main states of earth pressure: at-rest, active, and passive. The at-rest condition occurs when there is no lateral movement of the retaining wall. The coefficient of earth pressure at rest (K_0) is defined as:

$$K_0 = \frac{\sigma_h}{\sigma_v}$$

$K_p = \frac{1+\sin\phi}{1-\sin\phi}$

where σ_h is the lateral pressure and σ_v is the vertical pressure.

Active earth pressure develops when the wall moves away from the soil mass. For cohesionless soil, the active earth pressure coefficient (K_a) is given by:

from Mohr circle.

$$K_a = \tan^2(45 - \frac{\phi}{2}) = \frac{1-\sin\phi}{1+\sin\phi}$$

where ϕ is the internal friction angle of the soil.

Conversely, passive earth pressure occurs when the wall moves towards the soil mass. The passive earth pressure coefficient (K_p) for cohesionless soil is:

$$K_p = \tan^2(45 + \frac{\phi}{2})$$

For a cohesionless soil at depth z, the lateral pressures are calculated as:

$$\sigma_a = K_a \gamma z$$

$$\sigma_p = K_p \gamma z$$

where γ is the unit weight of the soil.

In 1915, Bell extended Rankine's theory to cohesive soils. For soils with cohesion (c), the total lateral earth pressures are given by:

$$\sigma_a = K_a \gamma z - 2c\sqrt{K_a}$$

$$\sigma_p = K_p \gamma z + 2c\sqrt{K_p}$$

Rankine's theory also predicts failure planes in the soil mass. In the active state, these planes make an angle of $(45 + f/2)$ with the horizontal, while in the passive state, the angle is (45° - φ/2).

Despite its widespread use, Rankine's theory has some limitations. It assumes no wall friction, which is often unrealistic. It's primarily applicable to walls with vertical backs and horizontal backfills. Additionally, the theory assumes the entire soil mass is in a state of plastic equilibrium, which may not always be true.

Despite these limitations, Rankine's lateral earth pressure theory remains a crucial tool in geotechnical engineering for the design of retaining walls and other earth-retaining structures. Its simplicity and ability to provide reasonable estimates make it a valuable starting point for many design calculations.

- Janssen's Janssen's equation, developed by H.A. Janssen in 1895, is a fundamental model in granular mechanics that describes the relationship between lateral pressure and normal stress in a cylindrical container filled with granular material. This equation provides crucial insights into the stress distribution within silos and similar structures, making it an essential tool in their design and analysis.

  The equation is based on several key assumptions. It considers the granular material to be cohesionless and assumes that the container walls are vertical and rigid. The model also posits that the ratio of horizontal to vertical stress (K) remains constant throughout the container, and that wall friction is fully mobilized. Additionally, it assumes a constant bulk density of the material.

  Mathematically, Janssen's equation for the vertical stress (σ_v) at a depth z in a cylindrical container is expressed as:

$$\sigma_v(z) = \frac{\gamma D}{4\mu K}\left(1 - e^{-\frac{4\mu K z}{D}}\right)$$

  In this equation, γ represents the bulk density of the granular material,

D is the container's diameter, μ is the coefficient of wall friction, K is the lateral pressure ratio, and z is the depth from the material's surface. The lateral pressure (σ_n) can then be calculated by multiplying the vertical stress by the lateral pressure ratio: $\sigma_h(z) = K\sigma_z(z)$.

This equation reveals several important characteristics of granular materials in containers. Unlike fluids, the stress in granular materials does not increase linearly with depth. Instead, there is a limiting stress as depth increases, known as the Janssen effect. Furthermore, the stress distribution is influenced by both the container's geometry and the material's properties.

Despite its widespread use, Janssen's equation has some limitations. It assumes a constant bulk density, which may not hold true for compressible materials. The assumption of fully mobilized wall friction may not always be valid, and the equation does not account for dynamic effects during filling or discharge of the container.

Notwithstanding these limitations, Janssen's equation remains a cornerstone in the design of silos and in understanding the behavior of granular materials. Its ability to predict stress distributions in static granular systems has made it an indispensable tool in various engineering applications, from agricultural storage to industrial processing of granular materials.

- Boussinesque Janssen's equation and Boussinesq's stress distribution are both important models in soil mechanics and granular materials, but they address different aspects of stress distribution in different contexts.

Janssen's equation, developed in 1895, describes the stress distribution in granular materials contained in silos or similar cylindrical structures. It accounts for the interaction between the granular material and the container walls, considering factors such as wall friction and the ratio of horizontal to vertical stress. Janssen's equation predicts that the vertical stress in a silo does not increase linearly with depth, but rather approaches a limiting value, known as the Janssen effect[4].

On the other hand, Boussinesq's equation, published in 1885, focuses on stress distribution in a semi-infinite, homogeneous, isotropic elastic medium due to a point load applied at the surface[1][5]. It is primarily used to calculate stresses at various depths and radial distances from the point of load application in soil mechanics.

- Boussinesq's equation for vertical stress (σz) at a point P at depth z due to a point load Q on the surface is given by:

$$\sigma_z = \frac{3Q}{2\pi z^2}\left[\frac{1}{1+\left(\frac{r}{z}\right)^2}\right]^{\frac{5}{2}}$$

  where:

  * Q is the magnitude of the point load
  * z is the vertical depth from the surface to point P
  * r is the horizontal distance from the point of load application to point P

This equation can also be expressed in terms of an influence factor (I_B), known as the Boussinesq stress coefficient:

$$\sigma_z = \frac{Q}{z^2} I_B$$

where:

$$I_B = \frac{3}{2\pi} \left[\frac{1}{1 + \left(\frac{r}{z}\right)^2} \right]^{\frac{5}{2}}$$

For the special case where r = 0 (directly beneath the point load), the equation simplifies to:

$$\sigma_z = \frac{3Q}{2\pi z^2}$$

Citations: [1] `https://civiltoday.com/geotechnical-engineering/soil-mechanics/144-boussinesqs-equation` [2] `https://testbook.com/civil-engineering/boussinesqs-equation-definition-and-hypothesis` [3] `https://testbook.com/question-answer/what-is-the-boussinesqs-vertical-stress-at-`

The key differences and relationships between these two models are:

1. Application context: Janssen's equation is specific to granular materials in confined spaces, while Boussinesq's equation applies to stress distribution in an elastic medium under surface loads.

2. Stress behavior: Janssen's equation predicts a non-linear increase in stress with depth, eventually reaching a limiting value. Boussinesq's equation

shows a continuous decrease in stress with depth and radial distance from the load point.

3. Material assumptions: Janssen's equation considers granular materials with friction, while Boussinesq's equation assumes a continuous, elastic medium.

4. Boundary conditions: Janssen's equation accounts for the presence of container walls, whereas Boussinesq's equation assumes an infinite medium in the horizontal direction.

5. Load type: Janssen's equation deals with the weight of the granular material itself, while Boussinesq's equation is used for external point loads applied at the surface.

While these models address different scenarios, they can be complementary in certain applications. For instance, in the design of foundations for silos or other structures on granular soils, engineers might use Boussinesq's equation to estimate stress distribution in the supporting soil, while Janssen's equation could be applied to calculate pressures within the silo itself.

It's important to note that both models have limitations and simplifying assumptions. In practice, more complex numerical methods or combined approaches may be necessary for accurate stress analysis in real-world scenarios involving both granular materials and elastic soil behavior.

Citations: [1] `https://civiltoday.com/geotechnical-engineering/soil-mechanics/144-boussinesqs-equation` [2] `https://www.cyut.edu.tw/~jrlai/CE7332/`

Chap8.pdf [3] https://www.rocscience.com/help/settle3/documentation/project-settings/stress-computation [4] https://www.sciencedirect.com/science/article/abs/pii/S0032591020311256 [5] https://testbook.com/civil-engineering/boussinesqs-equation-definition-and-hypothesis

4 Conclusions

From the observation that particles of corn cob show a larger standard deviation in the determined coefficient of friction, it can be hypothesized that particles of corn cob will have a high contribution to an erratic feedstock flow behavior. It can also be hypothesized that the cob will generate high frictional forces considering the high cohesive forces and moderate friction coefficients observed in a corn cob. The experimental data suggest that high-stress feedstock handling applications may be more stable with the removal of corn cob.

It is planned to repeat tests with variations in moisture content. High adhesive forces in cob particles containing 'woody-ring' subfractions may be reduced as moisture levels increase towards the fiber saturation point, but further studies are required to understand any adverse effects on friction coefficients.

The anatomical fractions discussed in this paper were categorized using macro-observations for the purpose of potential mechanical separation. Under further review, it appears each corn stover fraction contained an associated set of sub-fractions that could be found in at least one other fraction. Subfractions could be generally characterized as woody, pithy, or leafy. Additional steps in comminuting particles to expose 'sub-fractions' may allow fluid separation techniques to create more uniform and, therefore, desirable products. It is recommended to repeat this experiment using two additional comminution methods (i.e., knife mill and hammer mill) practiced in the industry to study varying effects of size reduction equipment on friction coefficients.

4.1 Future studies

Using DEM in biomass flow studies

5 Acknowledgment

This material is based upon work supported by the US Department of Energy's Office of Energy Efficiency and Renewable Energy (EERE) under the Bioenergy Technologies Office, Integrated Biorefinery Optimization award number DE-EE0008936.

This work was partially supported by USDA NIFA Agricultural Experiment Station project PEN-4671.

6 References

References

[1] G. Doyle, "Integrated Biorefinery Lessons Learned and Best Practices", in (July 2014), p. 13.

[2] USDOE, *U.S. Billion-Ton Update: Crop Residues and Agricultural Wastes* (Department of Energy, 2011).

[3] M. H. Langholtz, B. J. Stokes, and L. M. Eaton, *2016 Billion-Ton Report: Advancing Domestic Resources for a Thriving Bioeconomy*, DOE/EE-1440, ORNL/TM-2016/160, 1271651 (July 6, 2016), DOE/EE–1440, ORNL/TM–2016/160, 1271651.

[4] R. D. Perlack, L. M. Eaton, A. F. Turhollow Jr, M. H. Langholtz, C. C. Brandt, M. E. Downing, R. L. Graham, L. L. Wright, J. M. Kavkewitz, A. M. Shamey, et al., "US billion-ton update: biomass supply for a bioenergy and bioproducts industry", (2011).

[5] N. C. Crawford, N. Nagle, D. A. Sievers, and J. J. Stickel, "The effects of physical and chemical preprocessing on the flowability of corn stover", Biomass and Bioenergy **85**, 126–134 (2016).

[6] A. E. Ray, C. L. Williams, A. N. Hoover, C. Li, K. L. Sale, R. M. Emerson, J. Klinger, E. Oksen, A. Narani, J. Yan, C. M. Beavers, D. Tanjore, M. Yunes, E. Bose, J. H. Leal, J. L. Bowen, E. J. Wolfrum, M. G. Resch, T. A. Semelsberger, and B. S. Donohoe, "Multiscale Characterization of Lignocellulosic Biomass Variability and Its Implications to Preprocessing and Conversion: a Case Study for Corn Stover", ACS Sustainable Chemistry & Engineering **8**, 3218–3230 (2020).

[7] A. E. Ray, C. Li, V. S. Thompson, D. L. Daubaras, N. J. Nagle, and D. S. Hartley, *Biomass Blending and Densification: Impacts on Feedstock Supply*

and Biochemical Conversion Performance, Technical Report INL/MIS-16-38547-Revision-1 (Idaho National Laboratory (INL), Idaho Falls, ID, Feb. 22, 2017).

[8] T. L. Westover and D. S. Hartley, "Biomass Handling and Feeding", in *Advances in Biofuels and Bioenergy*, edited by M. Nageswara-Rao and J. R. Soneji (InTech, July 4, 2018).

[9] BETO, *Biorefinery Optimization Workshop Summary Report* (Department of Energy, Chicago, IL, 2016), p. 72.

[10] N. Kaliyan, R. V. Morey, M. D. White, and A. Doering, "Roll press briquetting and pelleting of corn stover and switchgrass", Transactions of the ASABE **52**, 543–555 (2009).

[11] H. A. Janssen, "Versuche uber getreidedruck in silozellen", Z. ver. deut. Ing. **39**, 1045 (1895).

[12] D. Schulze and J. Schwedes, "An examination of initial stresses in hoppers", Chemical Engineering Science **49**, 2047–2058 (1994).

[13] O. Reynolds, "LVII. On the dilatancy of media composed of rigid particles in contact. With experimental illustrations", `10.1080/14786448508627791` (1885).

[14] Y. Xia, T. Bhattacharjee, J. Klinger, E. Fillerup, J. Aston, and V. Thompson, "Defining Particle Size Distribution of Milled Biomass: Sieve Diameter versus Surface Area", in (July 2023), p. 12.

[15] F. Chen, Y. Xia, J. Klinger, and Q. Chen, "Hopper discharge flow dynamics of milled pine and prediction of process upsets using the discrete element method", Powder Technology **415**, 118165 (2023).

[16] F. Chen, Y. Xia, J. L. Klinger, and Q. Chen, "A set of hysteretic nonlinear contact models for DEM: Theory, formulation, and application for lignocellulosic biomass", Powder Technology **399**, 117100 (2022).

[17] ASTM G115-10, *Guide for Measuring and Reporting Friction Coefficients*, Standard, West Conshohocken, PA, 2018.

[18] J. Gao, W. D. Luedtke, D. Gourdon, M. Ruths, J. N. Israelachvili, and U. Landman, "Frictional Forces and Amontons' Law: From the Molecular to the Macroscopic Scale", The Journal of Physical Chemistry B **108**, 3410–3425 (2004).

[19] B. V. Derjaguin, "Molekulartheorie der äußeren reibung", Zeitschrift für Physik **88**, 661–675 (1934).

[20] B. V. Derjaguin, V. M. Muller, and Y. P. Toporov, "Effect of contact deformations on the adhesion of particles", Journal of Colloid and Interface Science **53**, 314–326 (1975).

[21] K. L. Kenney, W. A. Smith, G. L. Gresham, and T. L. Westover, "Understanding biomass feedstock variability", Biofuels **4**, 111–127 (2013).

[22] Z. Chen, C. Wassgren, and K. Ambrose, "Measurements of Grain Kernel Friction Coefficients Using a Reciprocating-Pin Tribometer", Transactions of the ASABE **63**, 675–685 (2020).

[23] B. V. Derjaguin and Y. P. Toporov, “Influence of adhesion on the sliding and rolling friction”, Progress in Surface Science **45**, 317–327 (1994).

[24] A. A. Pitenis, D. Dowson, and W. Gregory Sawyer, “Leonardo da Vinci’s Friction Experiments: An Old Story Acknowledged and Repeated”, Tribology Letters **56**, 509–515 (2014).